

# Machine learning with imaging features to predict the expression of ITGAV, which is a poor prognostic factor derived from transcriptome analysis in pancreatic cancer

YOSUKE IWATATE<sup>1\*</sup>, HAJIME YOKOTA<sup>2\*</sup>, ISAMU HOSHINO<sup>3</sup>, FUMITAKA ISHIGE<sup>1</sup>,  
NAOKI KUWAYAMA<sup>3</sup>, MAKIKO ITAMI<sup>4</sup>, YASUKUNI MORI<sup>5</sup>, SATOSHI CHIBA<sup>1</sup>,  
HIDEHITO ARIMITSU<sup>1</sup>, HIROO YANAGIBASHI<sup>1</sup>, WATARU TAKAYAMA<sup>1</sup>, TAKASHI UNO<sup>2</sup>, JASON LIN<sup>6</sup>,  
YUKI NAKAMURA<sup>6</sup>, YASUTOSHI TATSUMI<sup>6</sup>, OSAMU SHIMOZATO<sup>6</sup> and HIROKI NAGASE<sup>6</sup>

<sup>1</sup>Division of Hepato-Biliary-Pancreatic Surgery, Chiba Cancer Center, Chiba 260-8717; <sup>2</sup>Department of Diagnostic Radiology and Radiation Oncology, Graduate School of Medicine, Chiba University, Chiba 260-8670;

Divisions of <sup>3</sup>Gastroenterological Surgery and <sup>4</sup>Clinical Pathology, Chiba Cancer Center, Chiba 260-8717;

<sup>5</sup>Graduate School of Engineering, Faculty of Engineering, Chiba University, Chiba 263-8522;

<sup>6</sup>Laboratory of Cancer Genetics, Chiba Cancer Center Research Institute, Chiba Cancer Center, Chiba 260-8717, Japan

Received November 16, 2021; Accepted February 9, 2022

DOI: 10.3892/ijo.2022.5350

**Abstract.** Radiogenomics has attracted attention for predicting the molecular biological characteristics of tumors from clinical images, which are originally a collection of numerical values, such as computed tomography (CT) scans. A prediction model using genetic information is constructed using thousands of image features extracted and calculated from these numerical values. In the present study, RNA sequencing of pancreatic ductal adenocarcinoma (PDAC) tissues from 12 patients was performed to identify genes useful in evaluating clinical pathology, and 107 PDAC samples were immunostained to verify the obtained findings. In addition, radiogenomics analysis of gene expression was performed by machine learning using CT images and constructed prediction models. Bioinformatics analysis of RNA sequencing data identified integrin  $\alpha V$  (ITGAV) as being important for clinicopathological factors, such as metastasis and prognosis, and the results of sequencing and immunostaining demonstrated a significant correlation ( $r=0.625$ ,  $P=0.039$ ). Notably, the ITGAV high-expression group was associated with a significantly worse prognosis ( $P=0.005$ ) and recurrence rate ( $P=0.003$ ) compared with the low-expression group. The ITGAV prediction model showed

some detectability (AUC=0.697), and the predicted ITGAV high-expression group was also associated with a worse prognosis ( $P=0.048$ ). In conclusion, radiogenomics predicted the expression of ITGAV in pancreatic cancer, as well as the prognosis.

## Introduction

Pancreatic cancer is highly lethal with a poor prognosis, and no established sensitive markers for recurrence and survival. The overall 5-year survival rate is only 10% and increases to only 20% even after curative surgery; therefore, pancreatic cancer is considered one of the most fatal diseases (1-3). Large-scale genome analyses using next-generation sequencing (NGS) have been performed for pancreatic cancer (4) and subsequent transcriptome analyses have classified several RNA signatures (5,6).

Although recent technological developments have reduced the cost of gene research examination, such as gene sequencing, the economic costs and the time required for evaluation of the genetic information of each patient remain topics of debate. The field of radiogenomics has developed to evaluate genomic mutations and gene expression changes based on inexpensive and non-invasive general image data (radiomics); this field is currently attracting attention (7,8).

Images, such as those obtained by computed tomography (CT) and magnetic resonance imaging (MRI), are composed of quantitative digital data that are originally a collection of numerical values. The digital information obtained by such images can be quantified using mathematical methods by considering an image as a matrix of numbers. These quantitative values are called image features (IFs), and the field of study that deals with various IFs is called radiomics (9). Radiogenomics is expected to further facilitate the construction of models for predicting tumor molecular profiles by

*Correspondence to:* Dr Isamu Hoshino, Division of Gastroenterological Surgery, Chiba Cancer Center, 666-2 Nitona-cho, Chiba 260-8717, Japan  
E-mail: ihoshino@chiba-cc.jp

\*Contributed equally

**Key words:** pancreatic cancer, pancreatic ductal adenocarcinoma, radiogenomics, integrin  $\alpha V$ , machine learning, artificial intelligence

combining genomics techniques with radiomics-based analysis of image phenotypes, thereby allowing non-invasive, easy and inexpensive predictions.

The present study aimed to conduct a comprehensive search for molecules showing prognostic value for pancreatic cancer from the transcriptome, and to create a simple, inexpensive and non-invasive predictive model using these molecules and diagnostic imaging procedures commonly used for cancer treatment via radiogenomics analysis. In pancreatic cancer, numerous studies have comprehensively searched for factors associated with prognosis and recurrence using NGS and immunostaining (4-6). However, there are few reports that investigate the causal relationship between the results of gene expression determined by NGS and immunostaining; furthermore, there are few reports that have constructed predictive models from clinical images, such as CT images, in cases of pancreatic cancer (10). To the best of our knowledge, there is no report of such a causal relationship with regard to integrin  $\alpha$ V (ITGAV); therefore, this was the subject of the present study. To the best of our knowledge, no previous studies on various types of cancer have predicted the expression of ITGAV from CT images using radiogenomics analysis.

## Materials and methods

**Study population criteria.** A total of 143 patients were pathologically diagnosed with pancreatic cancer between January 2013 and March 2018 at Chiba Cancer Center following surgery. The average age of these patients was 68.7 years (46-87 years), 85 were men and 58 were women. Of these, patients who received preoperative chemotherapy, preoperative radiotherapy or preoperative chemoradiotherapy, or those that exhibited metastases to other organs were excluded. In addition, patients with cancer in other organs were excluded. Of the 143 patients, 107 satisfied the aforementioned conditions. Samples were retrospectively collected, and -fixed paraffin-embedded (FFPE) specimens were used in immunostaining, and frozen samples were used in RNA-seq in the present study. Of these cases, total RNA was extracted from a total of 15 cases, including six specimens that were collected intraoperatively and promptly frozen and nine frozen specimens stored in the biobank of Chiba Cancer Center, and comprehensively analyzed by NGS. The present study was approved by the Chiba Cancer Center Review Board (approval no. H29-006) and all patients provided written informed consent.

**RNA-sequencing (RNA-seq).** Total RNA was isolated from frozen tissue blocks containing 50-100 mg pancreatic ductal adenocarcinoma (PDAC) tissues or adjacent normal tissue. RNA was extracted using the miRNeasy Mini kit (cat. no. 217004; Qiagen, Inc.). The concentration of RNA was quantified using a NanoDrop system (NanoDrop; Thermo Fisher Scientific, Inc.). The quality of sufficiently concentrated samples was verified using the Agilent RNA 6000 Nano Kit (cat. no. 5067-1511; Agilent Technologies, Inc.). Samples with an RNA integrity number (RIN) value of  $\geq 7.0$  were used for RNA-seq. The loading concentration of the final library was measured using the Agilent High Sensitivity DNA kit (cat. no. 5067-4626; Agilent Technologies, Inc.)

and Agilent 2100 Bioanalyzer (Agilent Technologies, Inc.), and was 6 pM for RNA-seq. The library was built for NGS using Ion Total RNA-Seq kit v2 (cat. no. 4475936; Thermo Fisher Scientific, Inc.) and Ion Xpress™ RNA-Seq Barcode, cat. no. 4475485; Thermo Fisher Scientific, Inc.). RNA-seq was performed with an Ion Proton™ instrument (Thermo Fisher Scientific, Inc.). Sequencing data were mapped by Subread (<http://subread.sourceforge.net/>) to the hg19 reference genome. Differential expression levels were estimated by linear modeling based on LIMMA, a method of generating linear models for microarray data (11). Genes with a P-value of  $\leq 1.0 \times 10^{-4}$  were defined as differentially expressed genes (DEGs). Upon initial DEG analysis, the relative expression clustering profile patterns were assessed, and two pairs were excluded from further analysis based on the close proximity in expression patterns for the normal/tumor tissue pair with multidimensional scaling. After excluding 2 pairs, subsequent gene set enrichment analysis Gene Set Enrichment Analysis (GSEA; <https://www.gsea-msigdb.org/gsea/index.jsp>) and pathway analysis were performed using the Kyoto Encyclopedia of Genes and Genomes (KEGG; [https://www.genome.jp/kegg/kegg\\_ja.html](https://www.genome.jp/kegg/kegg_ja.html)). In addition, protein-protein interactions for the DEGs were analyzed and visualized using Cytoscape (ver. 3.8.1; <https://cytoscape.org/>) to identify the hub genes. The R2: Genomics Analysis and Visualization Platform (<https://hgserver1.amc.nl/cgi-bin/r2/main.cgi>) with expression and prognostic data (ID: PAAD; number of samples: 178) from The Cancer Genome Atlas Program was used to pre-verify whether these hub genes were associated with prognosis. Hub genes that exhibited a significant association with worsening prognosis in R2 underwent immunostaining.

**Immunohistochemical analysis.** The protein expression levels of ITGAV were measured by immunohistochemistry (IHC) using mouse monoclonal anti-human ITGAV protein antibody (P2W7; cat. no. sc-9969; 1:100; Santa Cruz Biotechnology, Inc.). Freshly removed pancreatic tissue samples were immediately fixed in 10% formalin for at least 24 h at 24°C and embedded in paraffin. Briefly, 5- $\mu$ m sections were obtained from FFPE tissues and underwent ITGAV staining with an OptiView DAB IHC Detection Kit (cat. no. 760-700; Roche Diagnostics) and a VENTANA BenchMark ULTRA automated slide stainer (Roche Diagnostics). A 3% hydrogen peroxide solution was used as the blocking reagent, and the sample was treated for 4 min at 36°C. Enzyme-induced antigen activation was performed using ISH Protease 1 (cat. no. 760-2018; Roche Diagnostics) for 32 min at 36°C, and the ITGAV primary antibody was applied to the sample for 120 min at 36°C to reduce non-specific reactions and background staining. According to the steps of the OptiView IHC Detection Kit, hydroxyquinoline was applied for 8 min at 36°C and then peroxidase-labeled anti-hydroxyquinoline mouse monoclonal antibody was applied as a secondary antibody for 8 min at 36°C. Finally, images were captured under a light microscope.

IHC results were scored based on the percentage positivity of staining. Two pathologists evaluated ITGAV protein expression as the percentage of the stained tumor cells and the stained area in the tumor interstitium. The staining intensity in the tumor cells and interstitium was also evaluated. The expression status of these proteins (low or high) was determined by

the percentage of tumor cells with any membrane staining, the staining area of interstitium and the staining intensity.

**IHC scoring of ITGAV and the related definitions.** Staining was usually observed in peripheral nerve cells in pancreatic tissue, and the staining levels in these areas were considered as controls. The percentage of tumor cells stained was scored as follows: 0, 0%; 1, 0–≤20%; 2, >20–≤40%; 3, >40–≤60%; 4, >60–≤80%; 5, >80%. The staining intensity of tumor cells was also scored (0–3) as follows: 0, none; 1, intensity lower than the control; 2, the same level as the control; 3, intensity higher than the control. The two scores, the percentage of stained tumor cells and the staining intensity of tumor cells, were multiplied and ITGAV expression in tumor cells was scored. Similarly, for tumor interstitial tissue, the proportion of staining in the interstitial area was calculated as follows: 0, 0%; 1, 0–≤20%; 2, >20–≤40%; 3, >40–≤60%; 4, >60–≤80%; 5, >80%. Staining intensity for the interstitial area was scored in the same manner as that for tumor cells. The two scores were then multiplied and to provide a score for ITGAV expression in the tumor interstitial tissue.

Finally, the IHC expression score of ITGAV in tumor tissues was calculated by adding the score in tumor cells to the score in tumor interstitial tissue. A regression line was created from this score using the least-squares method and RNA-seq expression, and a value higher than the IHC expression score, which corresponded to the median RNA expression, was regarded as high expression. Spearman's correlation coefficient analysis was used to examine the correlation between IHC expression scores and RNA-seq expression.

**Statistical analysis.** Continuous variables such as age were divided into two groups by median. The significant difference between ITGAV expression, and clinical and pathological variables was assessed using the  $\chi^2$  test, Fisher's exact test or Mann-Whitney U test. Overall survival (OS) was defined as the period between surgery and final observation (in days). Disease-free survival (DFS) was defined as the period between surgery and recurrence. A survival curve was prepared using the Kaplan-Meier method and the log-rank test was used to assess significant differences. Multivariate analysis was performed using the Cox regression model to determine significant factors in the log-rank test.  $P < 0.05$  was considered to indicate a statistically significant difference. These statistical analyses were conducted using JMP version 15.2.1 (SAS Institute, Inc.)

**CT acquisition and tumor segmentation.** CT scans were performed under the same conditions as our previous study, and a radiologist and a surgeon delineated the volume of interest-pancreatic cancer (VOI<sub>pc</sub>) (12). Subsequently, VOI<sub>+4 mm</sub> was created by mechanically expanding the axial plane by 4 mm around each VOI<sub>pc</sub>.

**IF extraction and machine learning.** IFs were extracted using the same protocol as that described in our previous study; the morphology, histogram and texture features were calculated from the original images (12). In addition, the same types of features were extracted from the original wavelet, Laplacian of Gaussian, square, square root, logarithm, exponential,

gradient, and local binary patterns in 2D- and 3D-filtered images. Finally, 3,748 (1,874x2) features were extracted from each VOI for early- and late-phase images. Feature selection consisted of two steps to stabilize the predictive power of the model. Firstly, Student's t-tests were performed on each IF, and only features with significant differences were retained, and another feature selection with recursive feature elimination was performed using a random forest function. Secondly, these IFs were input into extreme gradient boosting (XGBoost) to construct the predictive model for ITGAV. The feature selection and model construction steps were performed using nested cross-validation. Inner cross-validation for feature selection and outer cross-validation for model construction were five-fold. The probability of each sample was used for receiver operating characteristic (ROC) analysis. A ROC plot was created and the area under the curve (AUC) was calculated to evaluate the survival prediction of the machine learning models. The predicted status of ITGAV (high/low) was calculated using the predictive model and quantified in the range 0 to 1. These were arranged in descending order, divided into two groups near the actual ITGAV positive rate, the log-rank test was performed and several P-values were calculated; of these, the lowest P-value that would contribute most to survival and recurrence was adopted. All statistical analyses and machine learning were conducted using R version 3.5.1 (R Foundation for Statistical Computing) (Fig. 1).

## Results

**Patient background.** Between January 2013 and March 2018, a total of 143 patients were pathologically diagnosed with PDAC following surgery. Among of them, 119 patients underwent surgery without preoperative chemotherapy or radiation therapy, and were diagnosed with pancreatic cancer by postoperative pathological diagnosis. A total of 12 patients presented with cancer in other organs or with metastasis to other organs and were therefore excluded. As a result, a total of 107 cases were included in the present retrospective study. Specimens were available for a total of 15 patients. The Biobank provided frozen specimens for nine patients: Five cancer tissue specimens, and four matched cancer and normal tissue specimens. In addition, specimens for six other cases were obtained during the operation. The present study attempted to extract RNA from 10 pairs of cancerous and normal tissues, and five cancer tissues alone. Of the remaining 10 pairs, seven pairs passed the quality check with a RIN value of  $\geq 7.0$ , whereas two pairs showed RIN values of  $\geq 7.0$  for the cancer tissue only. All five cases in which only cancer tissues were collected exhibited RIN values of  $\geq 7.0$ . These cases underwent sequencing by NGS. Furthermore, the pairs of cancerous and normal tissues were evaluated on a multidimensional scale to assess whether they were valid. It was detected that one pair was likely to have been extracted only from cancerous tissue and another pair was likely to have been extracted only from normal tissue; therefore, two pairs were excluded (Fig. 2A). Finally, a total of 17 samples from 12 patients, including five pairs and seven cancer tissue samples, were available and analyzed for comprehensive total RNA bioinformatics analysis. RNA-seq analysis results were verified by IHC using the aforementioned 107 cases. The observation period was between January 2013

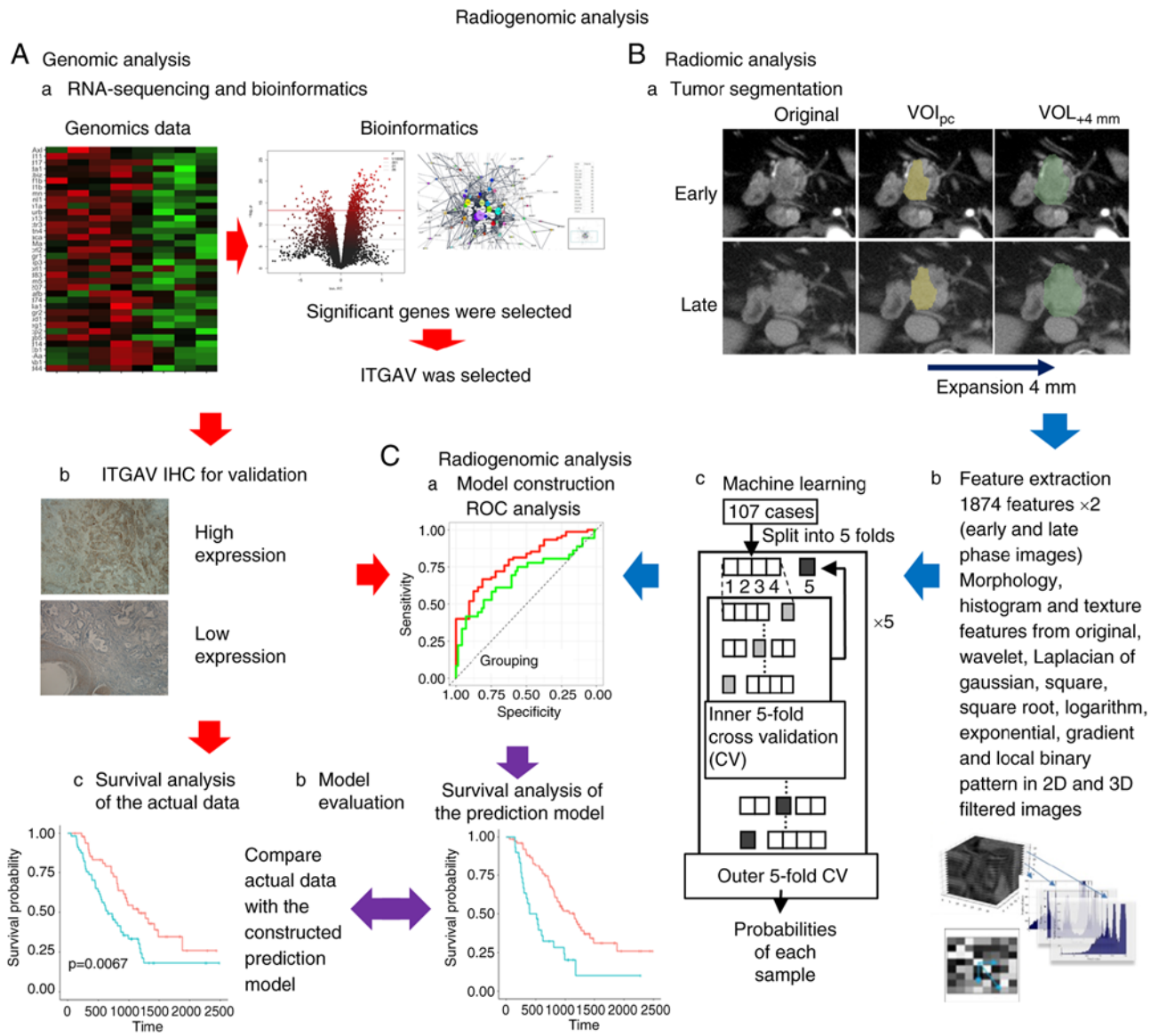


Figure 1. Schematic diagram of the present study was shown. (A-a) RNA-sequencing and bioinformatics was performed and ITGAV was detected as hub gene, which had clinically significant potential. (A-b) Group with high expression of ITGAV by IHC was evaluated for its association with clinicopathological factors. (A-c) Survival analysis was performed for ITGAV expression status using Kaplan-Meier analysis. (B-a) A region including the tumor region (VOI<sub>pc</sub>) and its surrounding 4 mm (VOI<sub>pc+4mm</sub>) was selected from the CT images. (B-b) Radiomics analysis was performed and IFs were extracted from CT. (B-c) A predictive model of ITGAV expression status was calculated from IF using extreme gradient boosting, which is a machine learning method. (C-a) A predictive model of high ITGAV expression was constructed from CT images using machine learning and evaluated with ROC plots. (C-b) The Kaplan-Meier curve of the predictive model was compared and evaluated with that of the actual one. IF, image feature; IHC, immunohistochemistry; ITGAV, integrin  $\alpha$ V; ROC, receiver operating characteristic; VOI<sub>pc</sub>, volume of interest pancreatic cancer.

and July 2020, with a median of 804 days (58-2,481 days). The median age was 70 years (50-87 years) and the male-to-female ratio was 60:47 (Table I).

**RNA-seq.** The expression levels were analyzed by mapping 11,272 mRNAs, and the number of DEGs whose expression fluctuated in cancer tissues in comparison with adjacent normal tissues was 314 (Fig. 2B). When these genes were analyzed by the KEGG pathway using GSEA, significant pathways included ECM-receptor interaction, focal adhesion, protein digestion, etc. (Table SI). When the degree of centrality in DEGs was calculated, the top 10 were examined to determine the relationship between gene expression and prognosis using the R2 platform, as follows: FN1 (P=0.147),

COL1A1 (P=0.098), COL1A2 (P=0.174), COL3A1 (P=0.206), COL5A1 (P=0.158), TIMP1 (P=0.041), COL4A1 (P=0.086), ITGB1 (P=0.036), FBN1 (P=0.131), COL5A2 (P=0.220), COL4A2 (P=0.121), SPARC (P=0.107), ITGAV (P=0.033) and MMP14 (P=0.093) (Fig. 2C). Of these, COL1A1, COL1A2, COL4A1, ITGB1, COL4A2 and ITGAV were mapped to the ECM-receptor interaction pathway. Of these mapped DEGs, high expression of ITGAV was significantly associated with poor prognosis (P=0.033, R2 platform; Fig. 2D); therefore, the clinicopathological significance of the ITGAV high expression group was verified by immunostaining.

**ITGAV IHC scoring.** For ITGAV, tumor cells had an IHC score of 0-18 (median, 8), tumor interstitial tissue had an IHC score



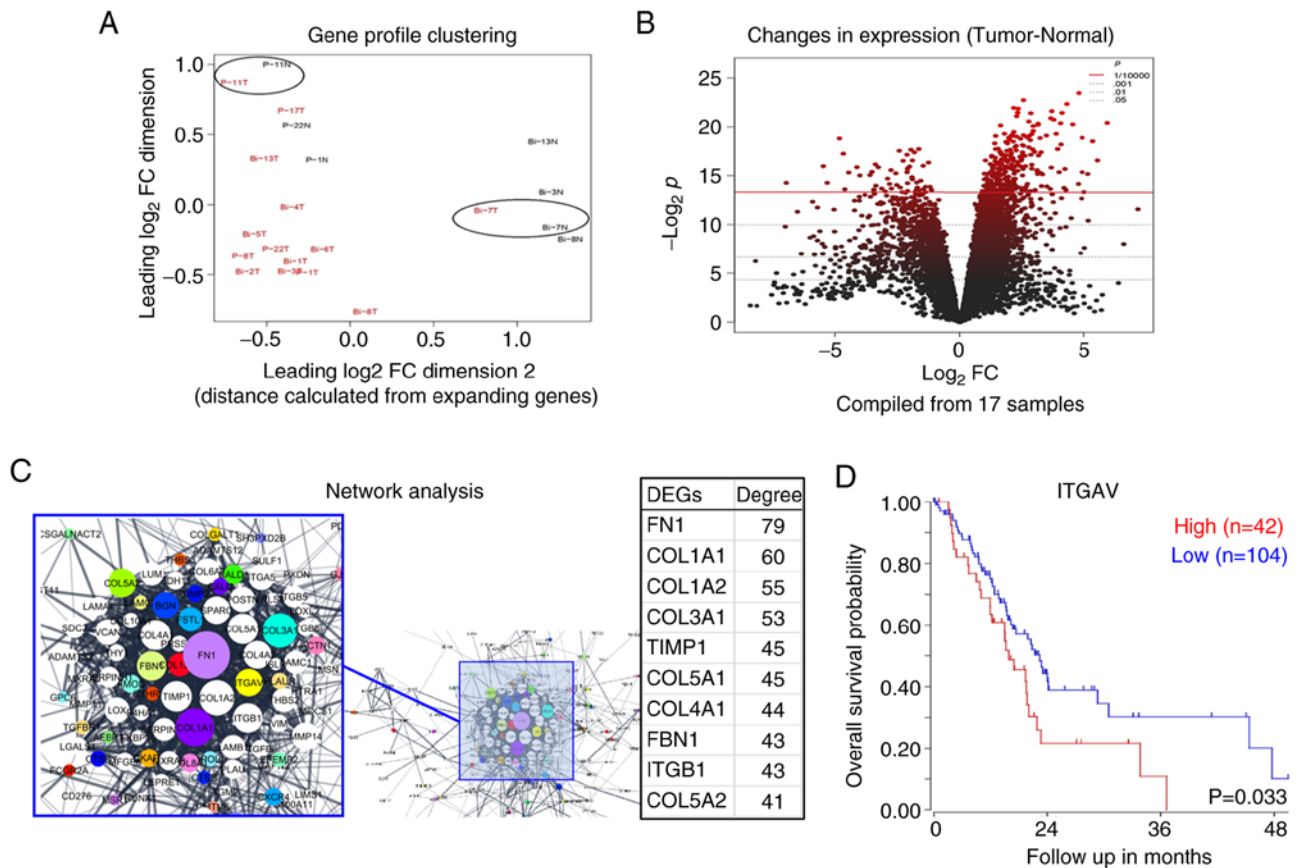


Figure 2. Bioinformatics analysis to identify genes that seemed to be clinically pathologically significant. (A) Multidimensional scaling plot of gene expression profiles from tissue specimens; horizontal and vertical axes as shown represent the first two dimensions, in which the largest variance between samples based on their relative root mean square deviations are typically expressed. The two pairs (shown circled in ellipses) were close proximal with this scaling and excluded from further analysis. (B) There were 314 differentially expressed genes that exhibited increased expression in cancer tissues than in normal tissues ( $P < 0.0001$ ). (C) Network analysis was performed on the interprotein relationships between mRNAs, and the top 10 hub genes with more central involvement were identified. (D) As a result of prognostic analysis with the R2 platform using The Cancer Genome Atlas data, ITGAV was revealed to be significantly associated with a worse prognosis ( $P = 0.033$ ), as determined by Kaplan-Miia analysis. ITGAV, integrin  $\alpha V$ .

of 0-15 (median, 0), and tumor tissue as a whole had an IHC score of 0-32 (median, 9) (Fig. 3A).

**Correlation between IHC scoring and RNA-seq.** With regard to ITGAV, there was a correlation between RNA-seq expression levels and tumor cell IHC scores, but there was no significant difference ( $r = 0.544$ ,  $p = 0.502$ ,  $P = 0.096$ ). Similarly, no significant correlation between RNA-seq expression levels and IHC scores was found in the interstitial tissue. However, there was a significant correlation between RNA-seq expression levels and IHC scores in the tumor tissue as a whole ( $r = 0.625$ ,  $p = 0.600$ ,  $P = 0.039$ ). According to the regression line, the IHC score which corresponded to the median RNA-seq expression level was 12.9; therefore, the optimal IHC score corresponding to the high expression of ITGAV by RNA sequencing was set to 13 (Fig. 3B).

**Association between IHC status and clinicopathological factors.** High ITGAV expression was observed in 25 cases (23.4%). No significant association was identified between ITGAV and sex or age (cutoff by median value, 70 years; range, 50-87 years). The high ITGAV expression group tended to have a larger tumor diameter (cutoff by median value, 3.3 cm; range, 1.0-11.6 cm) and contained significantly more T2 and T3 cases

( $P = 0.055$  and  $0.023$ , respectively). Other clinicopathological factors, such as preoperative tumor markers (CEA; cutoff by median value, 3.3 ng/ml; range, 0.5-47.3 ng/ml; and CA19-9; cutoff by median value, 137.4 U/ml; range, 0-47,588.2 U/ml) and lymph node metastases exhibited no significant differences (Table I).

**Relationship between clinicopathological factors and prognosis.** The presence of the tumor marker CA19-9 was associated with a significantly worse OS and DFS. Similarly, positive nerve infiltration, tumor diameter, T factor and lymph node metastasis also worsened OS and DFS. In addition, surgical procedure, operation time, bleeding volume, vascular infiltration, and postoperative adjuvant chemotherapy group were significantly associated with OS, and the histological type and lymphatic vessel infiltration were associated with DFS (Table II).

**Relationship between ITGAV expression status determined by IHC, prognosis and recurrence.** The present study investigated the relationship between prognosis and clinicopathological factors, including the expression status of ITGAV. In the ITGAV high-expression group, the prognosis was significantly worse alongside known prognostic factors, such as lymph node

Table I. Clinicopathological parameters and ITGAV status, as determined by immunohistochemistry.

Characteristic	ITGAV status		P-value
	Low, n (%)	High, n (%)	
Sex			0.353 <sup>a</sup>
Male	48 (44.9%)	12 (11.2%)	
Female	34 (31.8%)	13 (12.1%)	
Age, years <sup>d</sup>	69.5 (51-87)	71 (50-80)	0.777 <sup>b</sup>
Preoperative CEA, ng/ml <sup>d</sup>	3.25 (0.5-28.5)	3.4 (0.8-47.3)	0.779 <sup>b</sup>
Preoperative CA19-9, U/ml <sup>d</sup>	104.01 (0-47,588.2)	247.85 (0-31,800.7)	0.100 <sup>b</sup>
Operation type			0.690 <sup>c</sup>
Pancreatoduodenectomy	55 (51.4%)	15 (14.0%)	
Distal pancreatectomy	25 (23.4%)	10 (9.3%)	
Total pancreatectomy	2 (1.9%)	0 (0.0%)	
Cytology			0.621 <sup>a</sup>
Negative	72 (67.3%)	21 (19.6%)	
Positive	10 (9.3%)	4 (3.7%)	
Margin status			0.100 <sup>c</sup>
R0	68 (63.6%)	21 (19.6%)	
R1	12 (11.2%)	4 (3.7%)	
R2	2 (1.9%)	0 (0.0%)	
Differentiation			0.495 <sup>c</sup>
Well	37 (34.6%)	9 (8.4%)	
Moderate	38 (35.5%)	15 (14.0%)	
Poor	7 (6.5%)	1 (0.9%)	
Interstitium type			0.532 <sup>c</sup>
Medullary	1 (0.9%)	0 (0.0%)	
Intermediate	76 (71.0%)	22 (20.6%)	
Scirrhus	5 (4.7%)	3 (2.8%)	
Lymphatic invasion			0.690 <sup>a</sup>
Negative	23 (21.5%)	6 (5.6%)	
Positive	59 (55.1%)	19 (17.8%)	
Vascular invasion			0.579 <sup>a</sup>
Negative	1 (0.9%)	0 (0.0%)	
Positive	81 (75.7%)	25 (23.4%)	
Neural invasion			0.690 <sup>a</sup>
Negative	5 (4.7%)	1 (0.9%)	
Positive	77 (72.0%)	24 (22.4%)	
Lymph node metastasis			0.259 <sup>a</sup>
Negative	26 (24.3%)	5 (4.7%)	
Positive	56 (52.3%)	20 (18.7%)	
Max diameter, cm <sup>d</sup>	3.0 (1.0-10.0)	3.5 (1.3-7.0)	0.055 <sup>b</sup>
Postoperative adjuvant chemotherapy			0.374 <sup>a</sup>
Yes	19 (17.8%)	8 (7.5%)	
No	63 (58.9%)	17 (15.9%)	
pT (UICC) 8th			0.023 <sup>c</sup>
T1	18 (16.8%)	1 (0.9%)	
T2	47 (43.9%)	13 (12.1%)	
T3	17 (15.9%)	11 (10.3%)	

Table I. Continued.

Characteristic	ITGAV status		P-value
	Low, n (%)	High, n (%)	
pStage (UICC 8th)			0.210 <sup>c</sup>
IA	12 (11.2%)	0 (0.0%)	
IB	10 (9.3%)	4 (3.7%)	
IIA	4 (3.7%)	1 (0.9%)	
IIB	29 (27.1%)	8 (7.5%)	
III	27 (25.2%)	23 (21.5%)	

<sup>a</sup> $\chi^2$  test; <sup>b</sup>Mann-Whitney U test; <sup>c</sup>Fisher's exact test; <sup>d</sup>these data are presented as median (range). CA19-9, cancer antigen 19-9; CEA, carcino-embryonic antigen; ITGAV, integrin  $\alpha$ V; UICC, Union for International Cancer Control.

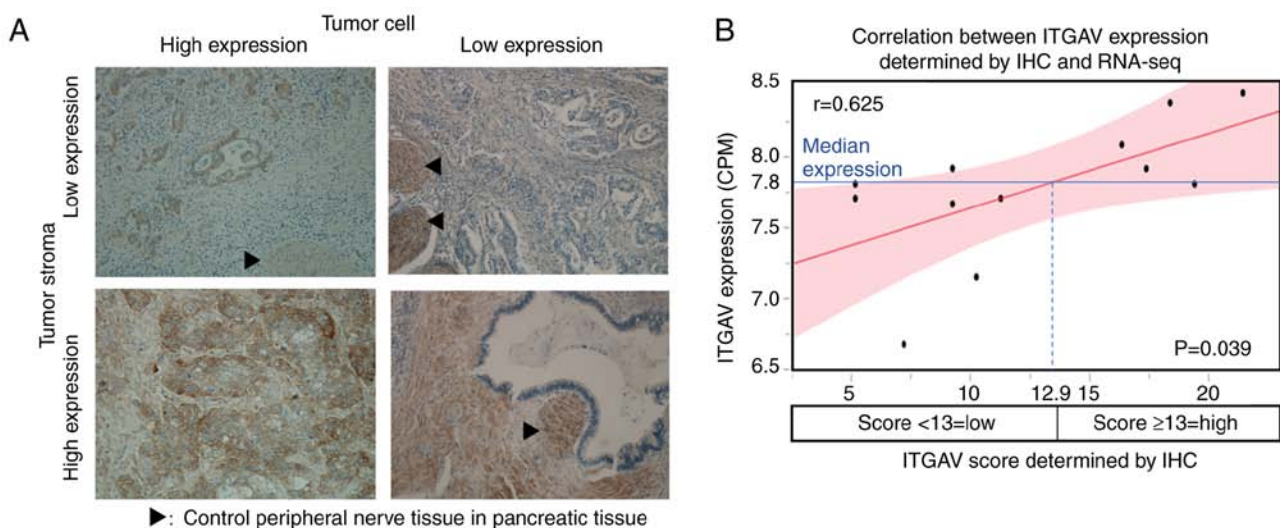


Figure 3. Typical ITGAV tissue staining and correlation between IHC expression score of ITGAV and RNA-seq expression. (A) For ITGAV, staining was usually observed in nerve tissue, and the levels of staining in these areas were considered as the control. The staining intensity, and staining area of the tumor interstitium and cancer cells differed from case to case. Magnification, x160. (B) There was a significant correlation between the RNA-seq expression levels and IHC scores of ITGAV in the tumor tissue ( $r=0.625$ ,  $\rho=0.600$ ,  $P=0.039$ ). A score exceeding IHC score of 13 was considered high expression of ITGAV;  $<13$  was considered low expression and  $\geq 13$  was considered high expression. IHC, immunohistochemistry; ITGAV, integrin  $\alpha$ V; RNA-seq, RNA sequencing.

metastasis, T factor and tumor markers. Similar to lymph node metastasis, tumor diameter and tumor markers, the ITGAV high-expression group also exhibited a significantly worsened recurrence rate (Table II).

**Evaluation of prognosis and recurrence predictors by multivariate analysis.** Among the 10 significant factors for OS in univariate analysis, tumor diameter was excluded because it has almost the same meaning as factor T (The Union for International Cancer Control; TNM Classification of Malignant Tumours, 8th Edition) (13). Multivariate analysis with the top seven of the 10 factors revealed that ITGAV, preoperative CA-19-9, surgical procedure, nerve infiltration, T factor and lymph node metastasis were independent prognostic factors (Table III). Similarly, multivariate analysis was performed on the eight significant factors for DFS as determined by univariate analysis, and revealed that ITGAV, neural invasion, T factor and lymph node metastasis were independent recurrence factors (Table III).

**Predictive power of machine learning models.** The AUC for ITGAV was 0.671 and 0.697 with imaging features of  $VOI_{pc}$  and  $VOI_{+4mm}$ , respectively (Fig. 4). Notably, OS was significantly different between the groups with predicted ITGAV from machine learning ( $P=0.048$ ). In terms of DFS, predicted high ITGAV expression was associated with a worse recurrence rate; however, this finding was not significant (Fig. 4).

## Discussion

The present study aimed to use CT images to predict the expression of ITGAV, which was confirmed to be an independent prognostic factor in pancreatic cancer using radiogenomics analysis. The results indicated that the expression of ITGAV could be predicted with appropriate sensitivity from CT images.

Integrin molecules consist of a dimer of an  $\alpha$  subunit and  $\beta$  subunit, and ITGAV forms  $\alpha$  subunits consisting of integrin  $\alpha$  chains (14). Integrin is a protein mainly present in the plasma membrane on the cell surface, which is involved in cell-cell

Table II. Univariate analysis of prognostic factors for OS and DFS.

Variable	No. of patients (%)	Univariate analysis for OS		Univariate analysis for DFS	
		Median, days (95% confidence interval)	Log-rank P-value	Median, days (95% confidence interval)	Log-rank P-value
Sex			0.527		0.760
Male	60 (56.1)	864 (622-1,065)		391 (260-575)	
Female	47 (43.9)	990 (494-1,324)		356 (223-498)	
Age, years			0.299		0.949
≤70	55 (51.4)	1,155 (730-1,276)		408 (282-561)	
>70	52 (48.6)	804 (515-963)		277 (247-458)	
Preoperative CEA, ng/ml			0.110		0.400
≤3.3	54 (50.0)	1,156 (730-1,324)		402 (279-737)	
>3.3	53 (50.0)	804 (572-911)		302 (225-458)	
Preoperative CA-19-9, U/ml			0.003		<0.001
≤137.4	54 (50.0)	1,175 (817-1,487)		594 (373-777)	
>137.4	53 (50.0)	572 (393-866)		252 (164-306)	
Operation type			0.007		0.113
PD	70 (65.4)	730 (534-942)		307 (256-455)	
DP/TP	37 (34.6)	1,324 (864-NA)		458 (263-832)	
Operation time, min			0.003		0.087
≤311	55 (51.4)	1,175 (817-1,512)		428 (298-641)	
>311	52 (48.6)	711 (515-911)		280 (243-498)	
Bleeding volume, ml			0.043		0.123
≤600	54 (50.5)	1,065 (746-1,512)		407 (282-575)	
>600	53 (49.5)	777 (560-990)		280 (243-498)	
Cytology			0.159		0.056
Negative	91 (88.3)	905 (746-1,175)		395 (298-526)	
Positive	12 (11.7)	454 (251-NA)		208 (106-484)	
Margin status			0.612		0.117
R0	86 (83.5)	864 (711-1,175)		356 (268-498)	
R1/R2	17 (16.5)	866 (455-1,212)		380 (135-575)	
Differentiation			0.055		0.035
Well	47 (43.9)	1,187 (800-1,512)		498 (282-839)	
Moderate/Poor	60 (56.1)	777 (534-963)		298 (243-408)	
Lymphatic invasion			0.122		0.001
Negative	29 (28.0)	1,243 (746-1,881)		746 (282-NA)	
Positive	78 (72.0)	817 (615-979)		304 (253-408)	
Neural invasion			0.022		0.020
Negative	6 (6.5)	NA (1,175-NA)		NA (280-NA)	
Positive	101 (93.5)	817 (656-990)		356 (263-458)	
Vascular invasion			0.039		0.147
Negative (v0/1)	21 (19.6)	1,512 (560-NA)		455 (279-1,064)	
Positive (v2/3)	85 (80.4)	823 (711-990)		356 (256-484)	
Interstitium type			0.223		0.807
Int	98 (91.6)	905 (735-1,156)		360 (279-484)	
Med + Sci	9 (8.4)	396 (248-1,881)		209 (57-NA)	
Max diameter, cm			0.033		0.003
≤3.3	57 (50.0)	1,155 (804-1,324)		561 (312-777)	
>3.3	50 (50.0)	711 (454-866)		263 (160-356)	



Table II. Continued.

Variable	No. of patients (%)	Univariate analysis for OS		Univariate analysis for DFS	
		Median, days (95% confidence interval)	Log-rank P-value	Median, days (95% confidence interval)	Log-rank P-value
Lymph node metastasis			<0.001		<0.001
Negative	31 (29.0)	1,512 (990-NA)		962 (455-NA)	
Positive	76 (71.0)	735 (534-866)		271 (209-373)	
T factor (UICC 8th)			0.010		0.024
T1/2	79 (76.7)	990 (804-1,276)		455 (302-641)	
T3	28 (26.2)	541 (304-864)		217 (144-343)	
Postoperative adjuvant chemotherapy			0.045		0.143
Yes	80 (74.8)	942 (804-1,243)		395 (298-526)	
No	27 (25.2)	599 (248-963)		225 (106-455)	
Stage (UICC 8th)			<0.001 <sup>a</sup>		<0.001 <sup>a</sup>
IA	12 (11.2)				
IB	14 (13.1)				
IIA	5 (4.7)				
IIB	37 (34.6)	1,187 [817-1,487 (I and II)]		498 [312-764 (I and II)]	
III	39 (36.4)	560 [362-823 (III)]		256 [160-386 (III)]	
ITGAV status			0.005		0.003
Low	82 (76.6)	1,065 (813-1,243)		441 (306-641)	
High	25 (23.4)	534 (287-804)		206 (119-302)	

<sup>a</sup>I and II vs. III. DFS, disease-free survival; DP, distal pancreatectomy; int, intermediate; ITGAV, integrin  $\alpha$ V; med, medullary; NA, not available; OS, overall survival; PD, pancreatoduodenectomy; sci, scirrhous; TP, total pancreatectomy; UICC, Union for International Cancer Control.

adhesion and signal transduction, and adhesion between cells, the extracellular matrix and the constructed extracellular micro-environment. ITGAV forms  $\alpha$  subunits, which form dimers with  $\beta$ 1,  $\beta$ 3,  $\beta$ 5,  $\beta$ 6 and  $\beta$ 8 (15-17). In addition, according to recent reports,  $\alpha$ V $\beta$ 3,  $\alpha$ V $\beta$ 5 and  $\alpha$ V $\beta$ 6 in tumor cells can activate TGF $\beta$  in cancer tissues, and TGF $\beta$  can induce  $\alpha$ V $\beta$ 6 and  $\alpha$ V $\beta$ 8 in pancreatic stellate cells in the tumor interstitium, causing interstitial changes that induce infiltration and metastasis (18,19).

High ITGAV expression has been reported to contribute to tumorigenesis, metastasis, proliferation and invasion in breast cancer, and high ITGAV expression has been observed in a group with nerve infiltration, lymph node metastasis and distant metastasis in colorectal cancer (20,21). In addition, high ITGAV expression in tumor cells has been shown to significantly shorten OS and DFS in gastric cancer and colon cancer; however, there are few reports of ITGAV in pancreatic cancer, and it was reported that no relationship existed between high ITGAV expression in tumor cells and prognosis (20,22,23). Regarding the interstitium, it has been reported that high ITGAV expression was detected in 48% of pancreatic stellate cells (PSCs) in the tumor interstitium (23). In the high expression group of ITGAV in PSCs in the tumor interstitium, the prognosis was significantly poor, and it was poor due to the high expression of ITGAV in PSCs in the peritumoral interstitium rather than in the tumor cells (23). The proportion of

high expression in tumor cells and peritumoral interstitium was generally consistent with the proportion in the present study (3,23,24). Furthermore, also in the present study, the high expression of ITGAV in tumor cells was not associated with prognosis ( $P=0.802$ ), whereas high expression of ITGAV in the entire tumor was associated with a worse prognosis. Therefore, high expression of ITGAV in pancreatic cancer tissue may contribute to high expression in the peritumoral environment, and ITGAV may reflect the malignant potential of the peritumoral environment rather than tumor cells.

For antitumor treatment, various integrin antagonists, such as  $\alpha$ V $\beta$ 3 and  $\alpha$ V $\beta$ 5, are in the development and research stage, and antitumor effects have been reported in breast cancer *in vitro* (20,25). In clinical trials using integrin inhibitors, there are currently no reports showing that a single agent is effective, but these agents are expected to be effective in combination with multiple agents, such as immune checkpoint inhibitors, and by case stratification (26). Although the effect of these agents in pancreatic cancer has not been reported, it is expected that ITGAV may contribute as a prognostic marker and treatment target in pancreatic cancer if the development, research, and clinical application of these integrin agents will progress in the future.

Radiogenomics analysis has extended to cancer of parenchymal organs, which yield easy to evaluate clinical

Table III. Multivariate analysis of prognostic factors for OS and DFS.

Variable	OS			DFS		
	Hazard ratio	95% confidence interval	P-value	Hazard ratio	95% confidence interval	P-value
Preoperative CA-19-9, U/ml						
≤137.4 (n=54)	1			1		
>137.4 (n=53)	1.761	1.065-2.932	0.028	1.717	0.981-3.020	0.058
Operation type						
PD (n=70)	1					
DP/TP (n=37)	0.393	0.199-0.768	0.006	NA		
Operation time, min						
≤311 (n=55)	1					
>311 (n=52)	1.027	0.547-1.883	0.930	NA		
Differentiation						
Well (n=47)				1		
Moderate/Poor (n=60)	NA			1.273	0.770-2.409	0.303
Lymphatic invasion						
Negative (n=29)				1		
Positive (n=78)	NA			1.805	0.875-3.999	0.112
Neural invasion						
Negative (n=6)	1			1		
Positive (n=101)	3.960	1.086-25.789	0.035	5.323	1.358-36.153	0.014
Lymph node metastasis						
Negative (n=31)	1			1		
Positive (n=76)	2.694	1.464-5.254	0.001	3.015	1.560-4.760	<0.001
T factor (UICC 8th)						
T1/2 (n=79)	1			1		
T3 (n=28)	2.326	1.317-4.014	0.004	2.126	1.171-3.794	0.014
ITGAV status						
Low (n=82)	1			1		
High (n=25)	1.873	1.048-3.247	0.035	2.152	1.168-3.329	0.015

DFS, disease-free survival; DP, distal pancreatectomy; ITGAV, integrin  $\alpha V$ ; OS, overall survival; PD, pancreatoduodenectomy; TP, total pancreatectomy; UICC, Union for International Cancer Control.

images, and to types of carcinoma with molecular markers for predicting drug effects, such as lung cancer, breast cancer and glioblastoma (9,27,28). Numerous studies have used radiomics to analyze the prognosis, and the presence or absence of lymph node metastasis from clinical images of pancreatic cancer, such as preoperative CT images. However, few radiogenomics reports have yielded molecular targets that can be evaluated from clinical images (10,29-31).

As aforementioned, high ITGAV expression has been reported to contribute to infiltration and metastasis in various types of cancer. In the present study, tumor diameter was increased in the ITGAV high-expression group and the T factor was more advanced. Therefore, high ITGAV expression may reflect peritumoral invasiveness in addition to changes in the extracellular microenvironment. These findings may indicate a tendency for early recurrence and deterioration of prognosis. Furthermore, in the radiogenomics analysis, the high expression

of ITGAV improved the detection ability in the analysis, including the tumor peripheral region ( $VOI_{+4\text{ mm}}$ ). These results may be reflected in the improvement of detection ability by including  $VOI_{+4\text{ mm}}$  in image evaluation (21). In addition, in the present study, evaluation using only CT images may be the cause of the insufficient ability to discriminate ITGAV status and predict the deterioration of the recurrence rate, and the detectability may be improved by using another modality, such as MRI.

The present study had limitations. RNA-seq was performed on a small number of cases, which may be insufficient to verify the correlation with IHC. Since this was a retrospective study at a single institution, the number of cases may have been insufficient to perform machine learning; because the number of cases was small, model creation and verification were performed in the same group. Therefore, model creation using more cases and verification at other facilities should be performed in the future.

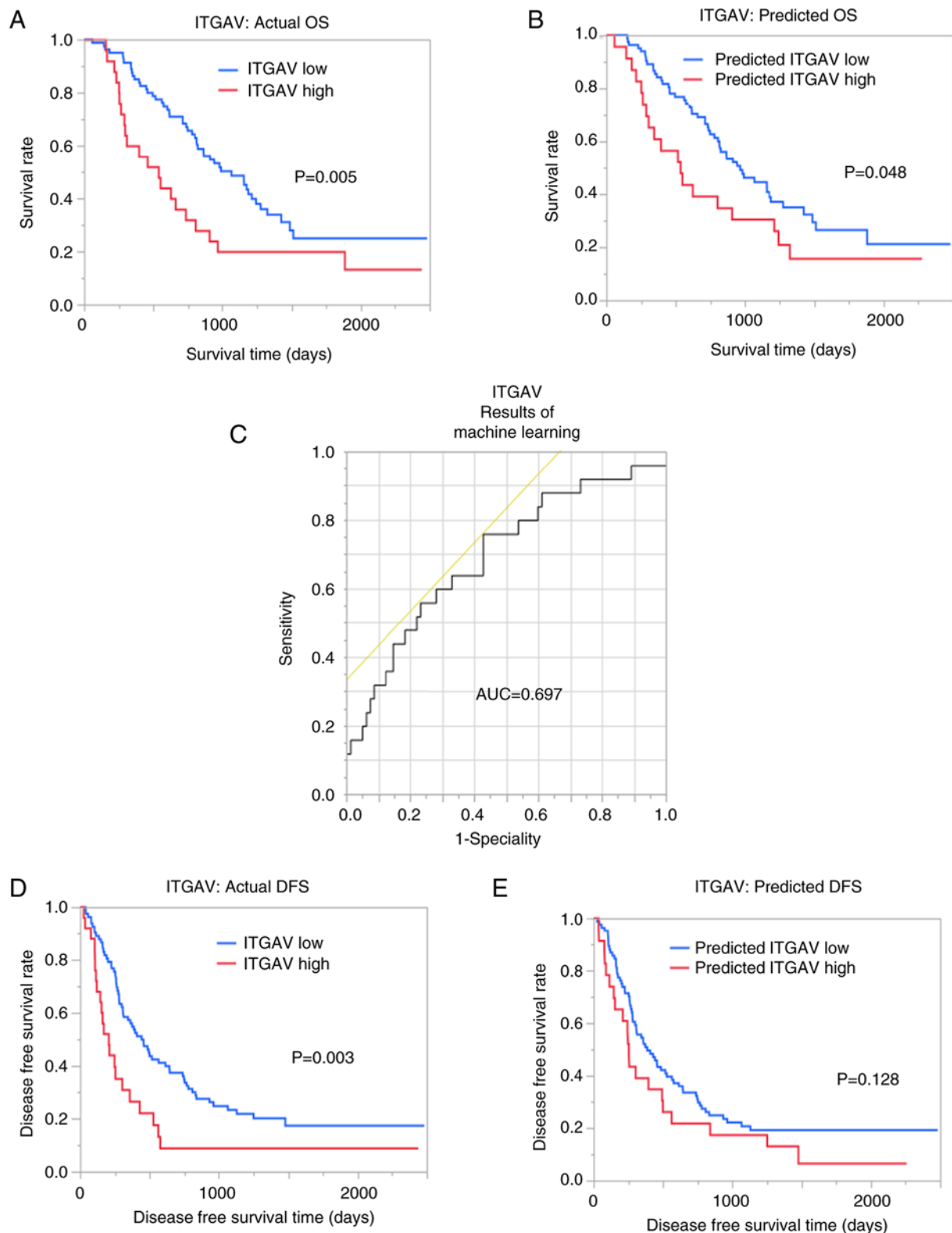


Figure 4. Comparison of ITGAV expression status by actual IHC and predictive model in overall survival and recurrence-free survival curve. (A) In OS, actual Kaplan-Meier curve of ITGAV status (high or low) and (B) the Kaplan-Meier curve of ITGAV status in the prediction model were shown. (C) Detectability for prediction model of ITGAV status from CT was shown by receiver operating characteristic curve (AUC=0.697). (D) In DFS, actual Kaplan-Meier curve of ITGAV status and (E) the Kaplan-Meier curve of ITGAV status in the prediction model were shown. The high ITGAV group calculated by the prediction model was significantly associated with OS, and was associated with DFS; however, this was not significant. AUC, area under the curve; DFS, disease-free survival; ITGAV, integrin  $\alpha$ V; OS, overall survival.

In conclusion, bioinformatics analysis of RNA-seq data for pancreatic cancer identified ITGAV as an important hub gene. Immunohistochemical staining with multiple samples revealed

that ITGAV expression was an independent predictor of prognosis and recurrence in multivariate analysis. Furthermore, high ITGAV expression with suggested clinical significance

and potential clinical application was predicted by machine learning using CT images.

## Acknowledgements

Not applicable.

## Funding

No funding was received.

## Availability of data and materials

The datasets used and/or analyzed during the current study are available from the corresponding author on reasonable request. The microarray data generated in the present study may be found in the Gene Expression Omnibus under accession number GSE196009 or at the following URL: <https://www.ncbi.nlm.nih.gov/geo/query/acc.cgi?acc=GSE196009>.

## Authors' contributions

YI, HY and IH analyzed and interpreted the patient data regarding pancreatic cancer, and wrote the manuscript. YI, IH and HN confirm the authenticity of all the raw data. HY and TU extracted imaging features from CT, and analyzed the relationship between imaging features and clinicopathological features. FI and NK performed RNA extraction. MI performed the pathological examination of the pancreatic cancer and interpreted the IHC results. YM examined the validity of the artificial intelligence in this study. SC, HA, HY and WT collected clinical pathological data. JL and HN performed bioinformatics analysis of RNA-seq data. YN, YT and OS created libraries from the extracted mRNA and sequenced them. HN oversaw this study comprehensively. All authors read and approved the final manuscript.

## Ethics approval and consent to participate

All patients provided written informed consent, and the study was approved by the Chiba Cancer Center Review Board (approval no. H29-006). All procedures were in accordance with the ethical standards of the responsible committee on human experimentation and with the Helsinki Declaration of 1964 and its later amendments.

## Patient consent for publication

Not applicable.

## Competing interests

The authors declare that they have no competing interests.

## References

- Mizrahi JD, Surana R, Valle JW and Shroff RT: Pancreatic cancer. *Lancet* 395: 2008-2020, 2020.
- Spath C, Nitsche U, Muller T, Michalski C, Erkan M, Kong B and Kleeff J: Strategies to improve the outcome in locally advanced pancreatic cancer. *Minerva Chir* 70: 97-106, 2015.
- Krüger K, Büning C and Schriever F: Activated T lymphocytes bind in situ to stromal tissue of colon carcinoma but lack adhesion to tumor cells. *Eur J Immunol* 31: 138-145, 2001.
- Waddell N, Pajic M, Patch AM, Chang DK, Kassahn KS, Bailey P, Johns AL, Miller D, Nones K, Quek K, *et al*: Whole genomes redefine the mutational landscape of pancreatic cancer. *Nature* 518: 495-501, 2015.
- Moffitt RA, Marayati R, Flate EL, Volmar KE, Loeza SG, Hoadley KA, Rashid NU, Williams LA, Eaton SC, Chung AH, *et al*: Virtual microdissection identifies distinct tumor- and stroma-specific subtypes of pancreatic ductal adenocarcinoma. *Nat Genet* 47: 1168-1178, 2015.
- Bailey P, Chang DK, Nones K, Johns AL, Patch AM, Gingras MC, Miller DK, Christ AN, Bruxner TJ, Quinn MC, *et al*: Genomic analyses identify molecular subtypes of pancreatic cancer. *Nature* 531: 47-52, 2016.
- Herskind C, Talbot CJ, Kerns SL, Veldwijk MR, Rosenstein BS and West CM: Radiogenomics: A systems biology approach to understanding genetic risk factors for radiotherapy toxicity? *Cancer Lett* 382: 95-109, 2016.
- Hoshino I and Yokota H: Radiogenomics of gastroenterological cancer: The dawn of personalized medicine with artificial intelligence-based image analysis. *Ann Gastroenterol Surg* 5: 427-435, 2021.
- Kickingereder P, Bonekamp D, Nowosielski M, Kratz A, Sill M, Burth S, Wick A, Eidel O, Schlemmer HP, Radbruch A, *et al*: Radiogenomics of glioblastoma: Machine learning-based classification of molecular characteristics by using multiparametric and multiregional MR imaging features. *Radiology* 281: 907-918, 2016.
- Attieyah MA, Chakraborty J, McIntyre CA, Kappagantula R, Chou Y, Askan G, Seier K, Gonen M, Basturk O, Balachandran VP, *et al*: CT radiomics associations with genotype and stromal content in pancreatic ductal adenocarcinoma. *Abdom Radiol (NY)* 44: 3148-3157, 2019.
- Ritchie ME, Phipson B, Wu D, Hu Y, Law CW, Shi W and Smyth GK: Limma powers differential expression analyses for RNA-sequencing and microarray studies. *Nucleic Acids Res* 43: e47, 2015.
- Iwatate Y, Hoshino I, Yokota H, Ishige F, Itami M, Mori Y, Chiba S, Arimitsu H, Yanagibashi H, Nagase H and Takayama W: Radiogenomics for predicting p53 status, PD-L1 expression, and prognosis with machine learning in pancreatic cancer. *Br J Cancer* 123: 1253-1261, 2020.
- Brierley JD, Gospodarowicz MK and Wittekind C (eds): TNM Classification of Malignant Tumours. Wiley, Chichester, 2017.
- Hynes RO: Integrins: Bidirectional, allosteric signaling machines. *Cell* 110: 673-687, 2002.
- Arcangeli A, Crociani O and Bencini L: Interaction of tumour cells with their microenvironment: Ion channels and cell adhesion molecules. A focus on pancreatic cancer. *Philos Trans R Soc Lond B Biol Sci* 369: 20130101, 2014.
- Desgrosellier JS and Cheresch DA: Integrins in cancer: Biological implications and therapeutic opportunities. *Nat Rev Cancer* 10: 9-22, 2010.
- Brown NF and Marshall JF: Integrin-Mediated TGF $\beta$  activation modulates the tumour microenvironment. *Cancers (Basel)* 11: 1221, 2019.
- Marsh D, Dickinson S, Neill GW, Marshall JF, Hart IR and Thomas GJ:  $\alpha$ 5 $\beta$ 6 Integrin promotes the invasion of morphoeic basal cell carcinoma through stroma modulation. *Cancer Res* 68: 3295-3303, 2008.
- Margadant C and Sonnenberg A: Integrin-TGF- $\beta$  crosstalk in fibrosis, cancer and wound healing. *EMBO Rep* 11: 97-105, 2010.
- Cheuk IW, Siu MT, Ho JC, Chen J, Shin VY and Kwong A: ITGAV targeting as a therapeutic approach for treatment of metastatic breast cancer. *Am J Cancer Res* 10: 211-223, 2020.
- Linhares MM, Affonso RJ Jr, Viana Lde S, Silva SR, Denadai MV, de Toledo SR and Matos D: Genetic and immunohistochemical expression of integrins ITGAV, ITGA6, and ITGA3 as prognostic factor for colorectal cancer: Models for global and disease-free survival. *PLoS One* 10: e0144333, 2015.
- Wang H, Chen H, Jiang Z, Lin Y, Wang X, Xiang J and Peng J: Integrin subunit  $\alpha$  V promotes growth, migration, and invasion of gastric cancer cells. *Pathol Res Pract* 215: 152531, 2019.

23. Horioka K, Ohuchida K, Sada M, Zheng B, Moriyama T, Fujita H, Manabe T, Ohtsuka T, Shimamoto M, Miyazaki T, *et al*: Suppression of CD51 in pancreatic stellate cells inhibits tumor growth by reducing stroma and altering tumor-stroma interaction in pancreatic cancer. *Int J Oncol* 48: 1499-1508, 2016.
24. Zhang B, Ye H, Ren X, Zheng S, Zhou Q, Chen C, Lin Q, Li G, Wei L, Fu Z, *et al*: Macrophage-expressed CD51 promotes cancer stem cell properties via the TGF- $\beta$ 1/smad2/3 axis in pancreatic cancer. *Cancer Lett* 459: 204-215, 2019.
25. Mattila E, Pellinen T, Nevo J, Vuoriluoto K, Arjonen A and Ivaska J: Negative regulation of EGFR signalling through integrin- $\alpha$ 5 $\beta$ 1-mediated activation of protein tyrosine phosphatase TCPTP. *Nat Cell Biol* 7: 78-85, 2005.
26. Alday-Parejo B, Stupp R and R  egg C: Are integrins still practicable targets for anti-cancer therapy? *Cancers (Basel)* 11: 978, 2019.
27. Woodard GA, Ray KM, Joe BN and Price ER: Qualitative radiogenomics: Association between oncotype DX test recurrence score and BI-RADS mammographic and breast MR imaging features. *Radiology* 286: 60-70, 2018.
28. Zhou M, Leung A, Echegaray S, Gentles A, Shrager JB, Jensen KC, Berry GJ, Plevritis SK, Rubin DL, Napel S and Gevaert O: Non-small cell lung cancer radiogenomics map identifies relationships between molecular and imaging phenotypes with prognostic implications. *Radiology* 286: 307-315, 2018.
29. Attiyeh MA, Chakraborty J, Doussot A, Langdon-Embry L, Mainarich S, G  nen M, Balachandran VP, D'Angelica MI, DeMatteo RP, Jarnagin WR, *et al*: Survival prediction in pancreatic ductal adenocarcinoma by quantitative computed tomography image analysis. *Ann Surg Oncol* 25: 1034-1042, 2018.
30. Liu P, Gu Q, Hu X, Tan X, Liu J, Xie A and Huang F: Applying a radiomics-based strategy to preoperatively predict lymph node metastasis in the resectable pancreatic ductal adenocarcinoma. *J Xray Sci Technol* 28: 1113-1121, 2020.
31. Xie T, Wang X, Li M, Tong T, Yu X and Zhou Z: Pancreatic ductal adenocarcinoma: A radiomics nomogram outperforms clinical model and TNM staging for survival estimation after curative resection. *Eur Radiol* 30: 2513-2524, 2020.



This work is licensed under a Creative Commons Attribution-NonCommercial-NoDerivatives 4.0 International (CC BY-NC-ND 4.0) License.